Modulation of the energetic electron distribution caused by toroidal mode ULF waves in association with periodic enhancement of whistler-mode chorus emissions

Atsuhiro Ono[1], Yuto Katoh[1], Mariko Teramoto[2], Tomoaki Hori[3], Atsushi Kumamoto[1], Fuminori Tsuchiya[1], Yasumasa Kasaba[1], Ko Isono[1], Yoshizumi Miyoshi[3], Satoshi Kasahara[4], Yoshiya Kasahara[5], Shoya Matsuda[5], Satoko Nakamura[3], Ayako Matsuoka[6], Shoichiro Yokota[7], Kunihiro Keika[4], Takefumi Mitani[8], and Iku Shinohara[9]

[1]Tohoku University
[2]Kyushu Institute of Technology
[3]Institute for Space-Earth Environmental Research, Nagoya University
[4]The University of Tokyo
[5]Kanazawa University
[6]Kyoto University
[7]Graduate School of Science, Osaka University
[8]ISAS/JAXA
[9]Japan Aerospace Exploration Agency

November 22, 2022

Abstract

ERG/Arase satellite observations show a simultaneous enhancement of whistler-mode chorus emissions and electron flux associated with toroidal mode ultra-low frequency (ULF) waves. The satellite observed the intensification of both chorus emissions and electron flux in the energy range satisfying the cyclotron resonance condition during the westward oscillation phase of the toroidal mode ULF waves. A model for the observed periodic variations is proposed. We consider the modulation of the drift speed of energetic electrons to be the drift due to the radial component of the wave electric field and the ambient magnetic field . Assuming a wave phase variation of the toroidal mode ULF oscillation in the azimuthal direction, we expect the accumulation of energetic electrons at locations corresponding to a specific phase angle, consistent with the observed phase relationship.

Modulation of the energetic electron distribution caused by toroidal mode ULF waves in association with periodic enhancement of whistler-mode chorus emissions

A. Ono[1], Y. Katoh[1], M. Teramoto[2], T. Hori[3], A. Kumamoto[1], F. Tsuchiya[1], Y. Kasaba[1],

K. Isono[1], Y. Miyoshi[3], S. Kasahara[4], Y. Kasahara[5], S. Matsuda[5], S. Nakamura[3],

A. Matsuoka[6], S. Yokota[7], K. Keika[4], T. Mitani[8], I. Shinohara[8]

[1]Graduate School of Science, Tohoku University, JAPAN

[2] Kyushu Institute of Technology, JAPAN

[3] Nagoya University, JAPAN

[4] University of Tokyo, JAPAN

[5] Kanazawa University, JAPAN

[6] Kyoto University, JAPAN

[7] Osaka University, JAPAN

[8] ISAS/JAXA, JAPAN

Corresponding author: Yuto Katoh (yuto.katoh@tohoku.ac.jp)

Key Points:

- ERG/Arase satellite observation of the simultaneous enhancement of whistler-mode chorus, toroidal mode ULF waves, and energetic electron flux
- Flux enhancement of 20-50 keV electrons is observed at the timing of the specific phase angle of the toroidal mode ULF waves
- A model for the modulation of the drift speed of energetic electrons by toroidal mode ULF waves is proposed

Abstract

ERG/Arase satellite observations show a simultaneous enhancement of whistler-mode chorus emissions and electron flux associated with toroidal mode ultra-low frequency (ULF) waves. The satellite observed the intensification of both chorus emissions and electron flux in the energy range satisfying the cyclotron resonance condition during the westward oscillation phase of the toroidal mode ULF waves. A model for the observed periodic variations is proposed. We consider the modulation of the drift speed of energetic electrons to be the $\boldsymbol{E}_X \times \boldsymbol{B}_\mathbf{0}$ drift due to the radial component of the wave electric field $\boldsymbol{E}_X$ and the ambient magnetic field $\boldsymbol{B}_\mathbf{0}$. Assuming a wave phase variation of the toroidal mode ULF oscillation in the azimuthal direction, we expect the accumulation of energetic electrons at locations corresponding to a specific phase angle, consistent with the observed phase relationship.

Plain Language Summary

Whistler-mode chorus emissions, interacting with energetic/relativistic electrons in the very wide energy range from a few keV to MeV, have been intensively studied for more than a half decade because of their significance in producing radiation belts and auroral electrons. Chorus emissions have been known by their periodic enhancement in the time scale of a few seconds to minutes, although physical processes governing the periodicity have not been fully understood. This paper analyses the ERG/Arase satellite observation of the simultaneous enhancements of both chorus emissions and electrons flux under the presence of toroidal mode ULF waves. The enhancement of both chorus emissions and electron flux is identified at a timing corresponding to the westward phase of the toroidal mode oscillations. We propose a model considering the

modulation of the drift speed of energetic electrons, which consistently explains the observed phase relationship between electrons and ULF waves.

1 Introduction

Whistler-mode chorus emissions play significant roles in the acceleration and the loss of energetic electrons in the terrestrial magnetosphere. Previous studies revealed that chorus emissions are generated through non-linear wave-particle interaction processes with energetic electrons (e.g., Omura et al., 2008, 2009; Omura, 2021). It was also revealed that chorus emissions cause the periodic precipitation of energetic electrons into the atmosphere through wave-particle interactions, contributing to diffuse and pulsating auroras (e.g., Coroniti and Kennel, 1970; Nishimura et al., 2010; Miyoshi et al., 2010, 2015, 2021; S. Kasahara et al., 2018a). While the mechanism controlling the periodicity of the chorus wave generation is one of the important problems unsolved in magnetospheric physics, the roles of ultra-low frequency (ULF) waves have been discussed for several decades. Previous studies focusing on the compressional ULF waves suggested that modulations of the linear growth rate of whistler-mode waves are responsible for the periodic enhancements of chorus emissions (e.g., Coroniti and Kennel, 1970; Li et al., 2011; Xia et al., 2016). The modulations of chorus emissions caused by poloidal and toroidal mode ULF waves are also reported (Jaynes et al., 2015; Liu et al., 2019; Zhang et al., 2019), while the modulation mechanism by only poloidal mode waves has been explained based on the drift resonance theory (e.g., Southwood and Kivelson, 1981). Although the roles of poloidal and compressional ULF waves have been revealed, it is still unclear how energetic electrons are modulated by toroidal mode waves. Based on the drift resonance theory, Elkington et al. (1999) discussed the modulation mechanism of MeV electrons caused by toroidal mode ULF waves assuming that the electron drift path is asymmetric between the noon sector and the midnight sector due to the compression of the magnetopause. However, how toroidal mode ULF waves can modulate the distribution of energetic electrons has not been fully understood. In the present study, we analyze substorm-related toroidal mode ULF waves, chorus emissions, and energetic electrons simultaneously observed by the Exploration of energization and Radiation in Geospace (ERG, also called Arase) satellite (Miyoshi et al., 2018a) and propose a model explaining how toroidal mode waves modulate energetic electrons.

2 Data and Instruments

The ERG satellite was launched on 20 December 2016 into an elliptical orbit with apogee and perigee altitudes of 32,000 km and 460 km, respectively, with an inclination angle of 31 degrees (Miyoshi et al., 2018a). We analyzed data obtained by the High Frequency Analyzer (HFA; Kumamoto et al., 2018; Y. Kasahara et al., 2018d), the Onboard Frequency Analyzer (OFA; Matsuda et al., 2018; Y. Kasahara et al., 2018c), and the Electric Field Detector (EFD; Kasaba et al., 2017; Y. Kasahara et al., 2018b) of the Plasma Wave Experiment (PWE; Y. Kasahara et al., 2018a), the Magnetic Field Experiment (MGF; Matsuoka et al., 2018a; Matsuoka et al., 2018b), the Medium-Energy Particle Experiments – Electron Analyzer (MEP-e; S. Kasahara et al., 2018b; S. Kasahara et al., 2018c) and the High-Energy Electron Experiments (HEP; Mitani et al., 2018a, 2018b, 2018c) aboard the ERG satellite, which were provided from the ERG science center (Miyoshi et al., 2018b).

The OFA processes signals in the frequency range from a few Hz to 20 kHz detected by both triaxial magnetic search coils (Ozaki et al., 2018) and two pairs of wire probe antennas (WPT; Kasaba et al., 2017) to produce frequency spectra and spectral matrices of wave electromagnetic fields. The HFA analyzed signals from WPT in the frequency range from a few kHz to 10 MHz to produce frequency spectra of the wave electric field. The HFA spectra are examined to determine the upper hybrid resonance (UHR) frequency and thereby estimate the plasma density by referring to the electron cyclotron frequency derived from the MGF measurements. The MGF measures the ambient magnetic field vector. The MEP-e provides the differential fluxes of electrons in the energy range from 7 to 87 keV. The HEP measures electrons in the energy range from 70 keV to 2 MeV. We used the wave electromagnetic field spectra, the ambient magnetic field vector, and the spin-averaged electron flux data with a time resolution of 8 s.

3 Results

We identified a simultaneous enhancement of both ULF waves and whistler-mode chorus emissions during the recovery phase of a magnetic storm on March 27, 2017, which was caused by the arrival of a corotating interaction region (CIR). The minimum Dst index for this storm was -74 nT. Figure 1 shows the time series of the solar wind parameters from 18:00 to 24:00 Universal Time (UT) on March 27, 2017. Figures 1(a)-(e) show the solar wind speed, dynamic pressure, proton density, and the z-component of the interplanetary magnetic field (IMF) in the Geocentric Solar Magnetospheric (GSM) coordinate system, and the AL index, respectively. Figure 1(a) indicates the arrival of the high-speed coronal hole stream (cf. Miyoshi and Kataoka, 2011), whose speed exceeds 600 km/s. The solar wind speed, the dynamic pressure, and the proton number density did not fluctuate significantly during this time interval (Figures 1a-c). On the other hand, Figure 1d shows Alfvénic fluctuations in the Z-component of IMF, contributing to the long-lasting intermittent enhancements of substorm activity (Figure 1e), a typical signature of CIR-driven storms (e.g., Tsurutani et al., 2006; Miyoshi et al., 2013). The AL index decreased to less than –1430 nT at 20:18 UT, indicating the development of an intense substorm.

We focus on the time interval from 21:30 UT to 22:00 UT, indicated by blue and red vertical lines in Figure 1. The ERG satellite was located in the range of McIlwain’s L-value (McIlwain, 1961) from 6.3 to 6.1, the magnetic local time from 04:00 to 04:12, and the magnetic latitude from -12.7 to -7.4 degrees. Figures 2(a) and (b) show the electric and magnetic field spectra, respectively, observed by OFA. The white and the red curves represent the local electron cyclotron frequency (f_{ce}) and 0.5 f_{ce}, respectively, derived from the total magnetic field intensity observed by MGF. We find periodic enhancements of lower-band chorus emissions with a period of ~2-3 minutes propagating parallel to the ambient magnetic field line (Figure S1). Figure 2(c) shows the time series of the magnetic field strength observed by the MGF, indicating the temporal variation from 145 nT to 130 nT with periodic fluctuations. Figures 2(d) and (e) show the time series of the three components of the magnetic field fluctuations observed by MGF in the Mean Field Aligned (MFA) coordinate system (cf. Takahashi et al., 1990), in which the Z component is taken toward the direction of the ambient magnetic field, $\boldsymbol{B_0}$, defined as the 200-s running averaged data of the magnetic field vector, the Y component is aligned to the direction of $\boldsymbol{B_0} \times \boldsymbol{r}$, where $\boldsymbol{r}$ is the position vector of the satellite taken from the center of the Earth, and the X component is taken in such a way that they form a right-handed orthogonal system, where the X- and Y-axes direct radially outward and eastward, respectively. Figure 2(d) represents the B_Z component of the magnetic field fluctuations, which dominates the fluctuation of the magnetic field intensity in this time interval shown in Figure 2(c), calculated by subtracting 200-s running averages from the time series of the Z-component of the magnetic field. In Figure 2(e), we find clear sinusoidal oscillations in the $B_{\boldsymbol{Y}}$ component and weaker oscillations in the $B_{\boldsymbol{X}}$ and $B_{\boldsymbol{Z}}$ components with periods similar to each other. The fluctuations in the $B_{\boldsymbol{Y}}$ component (green line in Figure 2e) reached over 5 nT in amplitude with a period of ~2-3 minutes. These results indicate that the observed periodic fluctuations in the magnetic field are toroidal mode Pc4-5 ULF waves. Since the time interval corresponds to the recovery phase of the strong substorm, the generation process of the observed ULF waves is thought to be related to the substorm. The comparison between Figures 2(a), (b), and (e) indicates the one-to-one correspondence between the observed chorus emissions and the toroidal mode ULF waves; chorus emissions are enhanced during the westward ($\Delta\mathrm{B}_{\boldsymbol{Y}} < 0$) phase of the toroidal mode oscillations. Figure 2(f) shows the X and Y components of the electric field in the MFA coordinate system measured by EFD, where we assume $\boldsymbol{E} \cdot \boldsymbol{B} = 0$ to obtain the electric field in the spin axis. The electric field also shows fluctuations of frequency similar to that of the magnetic field.

Figure 2(g) shows the omnidirectional electron number fluxes in the energy range from 12.0 keV to 87.5 keV measured by MEP-e. We find flux oscillations in the energy range of 35.0-60.4 keV. In order to examine these flux oscillations quantitatively, we calculate the residual flux (c.f. Claudepierre et al., 2013) given by $(J - J_0)/J_0$, where J and J_0 are the observed flux and its 200-s running average, respectively. Figure 2(h) shows the residual fluxes in the 35.0-60.4 keV energy range. The periodic oscillations in the residual fluxes are well correlated with both waveform of the ULF waves and the intensity of the chorus emissions; the fluxes of energetic electrons enhanced at the timings of the westward phase of the toroidal mode ULF wave oscillation and the enhancements of chorus emissions. Figure 2(i) shows the pitch angle distribution of the electron flux in the energy range from 48.3 keV to 52.3 keV. We find that the periodic enhancements of the electron flux in the pitch angle range perpendicular to the background magnetic field occurred at the timings closely correlated with the ULF waves and chorus emissions. Such periodic variations of the pitch angle distribution appear not only in the 50 keV but also in some neighboring energy ranges (Figure S2). The observed flux increase perpendicular to the magnetic field implies the enhancement of the temperature anisotropy of electrons.

4 Discussion and Summary

We showed the ERG satellite observation that the simultaneous enhancements of chorus emissions and electron flux occurred under the presence of the toroidal mode ULF waves. In order to understand the mechanism of the periodic enhancement of the observed chorus emissions, we analyzed the cyclotron resonance condition between whistler-mode waves and energetic electrons by referring to the plasma environment during the event. Previous studies suggest that chorus emissions are generated near the magnetic equator and then propagate away from the equator. Since the wave normal angle analysis by OFA shows that the observed chorus emissions propagated almost parallel to the ambient magnetic field line (Figure S1), we assume that the source region of the observed chorus emissions was located near the magnetic equator along a field line of the ERG satellite. We estimated parameters at the magnetic equator for the evaluation of the resonance condition. First, we computed the location of the equator along a field line of the satellite using the Tsyganenko-Sitnov 2005 model (Tsyganenko and Sitnov, 2005) with the observed solar wind data for the field line tracing and then estimated the ambient magnetic field intensity at the equator. Second, we estimated the plasma density to be 1.46 /cc at 21:40 UT and 1.96 /cc at 21:50 UT based on the UHR frequency identified in the spectra observed by HFA. Assuming that the plasma density is uniform along the magnetic field line from the location of the satellite to the magnetic equator, we used the estimated number density for the evaluation of the resonance condition. The first-order cyclotron resonance condition is considered for the resonant interaction between energetic electrons and whistler-mode waves propagating parallel to the background magnetic field. We estimated the resonant energies for a certain pitch angle of electrons for the time intervals of 21:40 UT and 21:50 UT. For the case of 0 degree pitch angle, the resonant energy is estimated to be 73-168 keV at 21:40 UT and 33-89 keV at 21:50 UT. In the case of 45 degree pitch angle, the resonant energy is estimated to be 132-293 keV at 21:40 UT and 62-161 keV at 21:50 UT. While significant periodic fluctuations do not appear in the electron flux for ~120-550 keV range observed by HEP (Figure S3), periodic fluctuations are evident in the electrons flux in the 35-60 keV range observed by MEP-e. Katoh et al. (2018) revealed by a series of electron hybrid code simulations that the condition required for the chorus generation is controlled by both the temperature anisotropy and the number density of energetic electrons. A certain level of the number density of energetic electrons is required for the chorus generation. They also showed that the required number density of energetic electrons lowers for higher temperature anisotropy. The enhancement of the electron flux in the pitch angle range perpendicular to the background magnetic field shown in Figure 2 provides favorable conditions for chorus generation. The observation results suggest that the toroidal mode ULF waves play an important role in forming the favorable condition for the enhancements of chorus emissions.

The intensities of chorus emissions and electron flux in the 50 keV energy range, satisfying the cyclotron resonance condition, are enhanced during the negative (westward) phase of the toroidal mode oscillations. Figure 3(a) illustrates the phase relationship between the electromagnetic field waveforms of the toroidal mode ULF waves and the flux of energetic electrons. Figures 2e-f showed that the radial component of the wave electric field (E_X) delays by 90 degrees in phase from the azimuthal component of the magnetic field (B_Y). The phase relation between the wave electromagnetic fields observed by the ERG satellite located in the southern hemisphere suggests that the observed ULF waves are second harmonic standing waves (cf. Takahashi et al., 1996; 2011). Spectra of the waveform in the electric field indicate that the fundamental mode is also present; the wave amplitude of the fundamental mode is ~2 mV/m.

The oscillation of E_X results in the variation of the $\boldsymbol{E}_X \times \boldsymbol{B}_0$ drift speed depending on the wave phase of the ULF wave as shown in Figure 3(a), where the labels (A) to (E) represent the wave phase every $\pi/2$. The observation result revealed that the residual flux of energetic electrons maximizes at the minimum of the B_Y waveform, as illustrated in Figure 3(a).

We consider a possible mechanism causing the distribution of energetic electrons localized at a specific phase angle of toroidal mode ULF waves. Let us assume the spatial variation of the wave phase of the toroidal mode ULF oscillation in the azimuthal direction. Considering that the wave phase increases eastward (+Y in the MFA coordinates) and that the phase relationship shown in Figure 3(a) is the spatial structure locally formed in the inner magnetosphere, a model for the observed periodic flux variations can be proposed as follows. Let us convert the time series of the waveforms shown in Figure 3(a) into a spatial structure on the equatorial plane of the magnetosphere as indicated in Figure 3(b); the wave phases corresponding to (A)-(E) in Figure 3(a) can be placed azimuthally clockwise along the electron drift path, as shown in Figure 3(b). The $\boldsymbol{E}_X$ and the $\boldsymbol{E}_X \times \boldsymbol{B}_0$ drift velocity vectors at locations (A) to (E) are also shown. Figure 3(b) indicates that the modulation of the $\boldsymbol{E}_X \times \boldsymbol{B}_0$ drift due to the toroidal mode ULF waves tend to converge/diverge energetic electrons azimuthally; the $\boldsymbol{E}_X \times \boldsymbol{B}_0$ around (D) converges electrons toward (D) and around (B) sweeps electrons away from (B). Thus, we expect the enhancement of the electron flux at the specific wave phase of the toroidal mode ULF waves corresponding to (D). In Figure 2(h), the rectangular variation of the residual flux with a single peak is found at 21:42 during the westward oscillation phase of the B_Y waveform, similar to Figure 3(a). The residual flux in the time interval from 21:44 to 21:53 also maximizes during the westward oscillation phase of B_Y, but the variation is sinusoidal rather than rectangular. The sinusoidal variation may indicate a transition stage of the convergence of the electron flux due to the ULF waves. A rectangular flux variation with a single peak can be expected in an ideal case that electrons around (B) in Figure 3(a) are completely swept out and fully converged around (D). A sinusoidal flux variation can be expected during a transition stage forming a flux peak around (D) with a depletion around (B), corresponding to the eastward oscillation phase of B_Y. Since a single peak of the flux variation indicated in Figure 3 requires an ideal situation, sinusoidal variation would be typical in the magnetosphere.

Considering that the spatial structure formed by the regions of the enhanced electron flux moves with the wave phase variation of the ULF waves, we expect that the whole spatial structure drifts eastward with the phase velocity of the ULF wave. Then we can reconstruct the time series of the waveforms (Figure 3a) from the spatial distribution (Figure 3b); the flux enhancement is observed by the satellite at the timings corresponding to the wave phase angle corresponding to (D) in Figure 3(a). This model suggests that the dense region caused by the azimuthal inhomogeneity of the $\boldsymbol{E}_X \times \boldsymbol{B}_\mathbf{0}$ drift corresponds to the flux enhancement observed by the ERG satellite.

The flux enhancement of the proposed model becomes significant in a case where the $\boldsymbol{E}_X \times \boldsymbol{B}_\mathbf{0}$ drift speed is comparable to the magnetic drift speed of energetic electrons. We estimate the $\boldsymbol{E}_X \times \boldsymbol{B}_\mathbf{0}$ drift speed from the electric and magnetic field data observed by EFD and MGF. According to the ULF amplitude in the electric field of 2 mV/m and the background magnetic field intensity of 130 nT, the $\boldsymbol{E}_X \times \boldsymbol{B}_\mathbf{0}$ drift speed is estimated to be about 15.4 km/s. On the other hand, the bounce averaged drift period $\langle \tau_d \rangle$ [sec] of energetic electrons in the dipole field is given by (cf. Walt, 1994)

$$\langle \tau_d \rangle = \frac{\pi e B_E R_E^2}{LW}\left[1 - \frac{1}{3}\left(\sin \alpha_{eq}\right)^{0.62}\right], \quad (1)$$

where e is the elementary charge, B_E is the equatorial magnetic field intensity on the surface of the Earth, about 31,100 nT, R_E is the Earth's radius, L is L-value, W and α_{eq} are the kinetic energy and the equatorial pitch angle of electrons, respectively. The drift speed V_B of electrons of the 90 degree pitch angle is given by

$$V_B = \frac{2\pi L R_E}{\langle \tau_d \rangle} = \frac{2W}{eB_E}\frac{L^2}{R_E}. \quad (2)$$

Then V_B of electrons in the energy range of 35-60 keV at L=6 is estimated to be 12.3-20.7 km/s, comparable to the estimated $\boldsymbol{E}_X \times \boldsymbol{B}_0$ drift speed. Since the bounce period is much shorter than both the time scale of the drift motion of energetic electrons and the wave period of the observed ULF waves, we can neglect the azimuthal motion of energetic electrons during one bounce period. The bounce period τ_b [sec] of energetic electrons in the dipole field is given by (cf. Walt, 1994)

$$\tau_b = 0.117\, L\frac{c}{v}\left[1 - 0.4635\left(\sin \alpha_{eq}\right)^{3/4}\right], \quad (3)$$

where v denotes the speed of electron and c represents the speed of light. For electrons of the 60 degree pitch angle in the energy range of 35-60 keV, τ_b is estimated to be 0.16-0.2 seconds.

In the higher latitude region away from the equator, where bouncing electrons spend most of the bouncing period, the effects of the azimuthal inhomogeneity of the $\boldsymbol{E}_X \times \boldsymbol{B}_0$ drift speed on energetic electrons are thought to be weaker because the ambient magnetic field intensity is stronger and the $\boldsymbol{E}_X \times \boldsymbol{B}_0$ drift speed is slower. The electric field of the fundamental mode at the equator should be larger than those observed. Thus, the amplitude of the flux variation of bouncing electrons is thought to be smaller than that of near-equatorially mirroring electrons. Although quantitative evaluation should be performed in our future study, this difference in the flux variation according to the equatorial pitch angle may cause the observed pitch angle dependence of energetic electrons shown in Figure 2(i).

Finally, we discuss the spatial scale of the interaction region associated with the ULF waves, chorus emissions, and energetic electrons. The proposed model suggests that the azimuthally localized electron structure is drifting eastward with the phase velocity of ULF waves. The longitudinal wavelength is estimated to be 2,310 km using the wave period 150 sec and the drift speed of 15.4 km/s, corresponding to the m number of ~17. Although the estimated spatial scale is smaller than those of the externally excited toroidal mode ULF waves typically observed in the inner magnetosphere [cf. Takahashi, 2016] and is rather comparable to those of internally driven poloidal mode ULF waves, previous studies reported eastward-propagating internally driven ULF waves with a similar azimuthal wavenumber during a substorm [James et al., 2013; Hori et al., 2018]. Validation of the proposed scenario on the modulation of energetic electrons by toroidal mode ULF waves should be conducted by a statistical survey of the data and by numerical simulations, which are left for future studies.

Data Availability Statement

The present study analyzed PWE/OFA L2-v02_02 data (doi:10.34515/DATA.ERG-08000), PWE/EFD L2-v05_01 data (doi:10.34515/DATA.ERG-07000), PWE/HFA L2-v01_02 data (doi:10.34515/DATA.ERG-10000), MGF-L2 8 sec spin-averaged data v03_04 (doi:10.34515/DATA.ERG-06001), MEP-e-L2 3-D flux data v01_01 (doi:10.34515/DATA.ERG-02000), MEP-e-L2 omniflux data v01_02 (doi:10.34515/DATA.ERG-02001), HEP-L2 omniflux data v03_01 (doi:10.34515/DATA.ERG-01001), HEP-L3 pitch angle sorted electron flux data v01_01 (doi:10.34515/DATA.ERG-

01002), and Orbit L2 v03 data (doi:10.34515/DATA.ERG-12000). The SPEDAS software (Angelopoulos et al., 2019) and ERG Plug-in tools were used for data analysis.

Acknowledgments

This study is supported by Grants-in-Aid for Scientific Research (15H05747, 18H03727, 20H01959, and 20K04052) of Japan Society for the Promotion of Science. This research is also supported by the joint research program of the Institute for Space-Earth Environmental Research, Nagoya University.

References

Angelopoulos, V., Cruce, P., Drozdov, A., Grimes, E. W., Hatzigeorgiu, N., King, D. A., et al. (2019) The Space Physics Environment Data Analysis System (SPEDAS), Space Sci. Rev., 215, 9, doi:10.1007/s11214-018-0576-4.

Baumjohann, W., and R. A. Treumann (1996), ”Basic Space Plasma Physics”, London, Imperial College Press.

Claudepierre, S. G., I. R. Mann, K. Takahashi, J. F. Fennell, M. K. Hudson, J. B. Blake, J. L. Roeder, J. H. Clemmons, H. E. Spence, G. D. Reeves, D. N. Baker, H. O. Funsten, R. H. W. Friedel, M. G. Henderson, C. A. Kletzing, W. S. Kurth, R. J. MacDowall, C. W. Smith, and J. R. Wygant (2013), Van Allen Probes observation of localized drift resonance between poloidal mode ultra-low frequency waves and 60 keV electrons, *Geophys. Res. Lett.*, 40, 4491–4497, doi: 10.1002/grl.50901.

Coroniti, F. V., and C. F. Kennel (1970), Electron Precipitation Pulsations, *J. Geosphys. Res.*, 75, 1279-1289.

Elkington, S. R., M. K. Hudson, and A. A. Chan (1999), Acceleration of relativistic electrons via drift-resonant interaction with toroidal-mode Pc-5 ULF oscillations, *Geophys. Res. Lett.*, 26, 3273-3.

Hori, T., N. Nishitani, S. G. Shepherd, J. M. Ruohoniemi, M. Connors, M. Teramoto, S. Nakano, K. Seki, N. Takahashi, S. Kasahara, S. Yokota, T. Mitani, T. Takashima, N. Higashio, A. Matsuoka, K. Asamura, Y. Kazama, S.-Y. Wang, S. W. Y. Tam, T.-F. Chang, B.-J. Wang, Y. Miyoshi, I. Shinohara (2018), Substorm-Associated Ionospheric Flow Fluctuations During the 27 March 2017 Magnetic Storm: SuperDARN-Arase Conjunction, Geophys. Res. Lett., 45, 18, 9441-9449, doi:10.1029/2018GL079777.

Hori, T., T. Mitani, A. Matsuoka, M. Teramoto, I. Park, T. Takashima, Y. Miyoshi, and I. Shinohara (2020), The HEP instrument Level-3 pitch angle sorted electron flux data of Exploration of energization and Radiation in Geospace (ERG) Arase satellite, DOI:10.34515/DATA.ERG-01002.

James, M. K., T. K. Yeoman, P. N. Mager, D. Yu. Klimushkin (2013), The spatio-temporal characteristics of ULF waves driven by substorm injected particles, J. Geophys. Res. Space Phys., 118, 4, 1737-1749, doi:10.1002/jgra.50131.

Jaynes, A. N., M. R. Lessard, K. Takahashi, A. F. Ali, D. M. Malaspina, R. G. Michell, E. L. Spanswick, D. N. Baker, J. B. Blake, C. Cully, E. F. Donovan, C. A. Kletzing, G. D. Reeves, M. Samara, H. E. Spence, and J. R. Wygant (2015), Correlated Pc4–5 ULF waves, whistler-mode chorus and pulsating aurora observed by the Van Allen Probes and ground-based systems, *J. Geosphys. Res.*, 120, 8749–8761, doi:10.1002/2015JA021380.

Kasaba, Y., K. Ishisaka, Y. Kasahara, T. Imachi, S. Yagitani, H. Kojima, S. Matsuda, M. Shoji, S. Kurita, T. Hori, A. Shinbori, M. Teramoto, Y. Miyoshi, T. Nakagawa, N. Takahashi, Y. Nishimura, A. Matsuoka, A. Kumamoto, F. Tsuchiya, and R. Nomura (2017), Wire Probe Antenna (WPT) and Electric Field Detector (EFD) of Plasma Wave Experiment (PWE) aboard the Arase satellite: specifications and initial evaluation results, *Earth Planets Space*, 69, 174, doi:10.1186/s40623-017-0760-x.

Kasahara, S., Y. Miyoshi, S. Yokota, T. Mitani, Y. Kasahara, S. Matsuda, A. Kumamoto, A. Matsuoka, Y. Kazama, H. U. Frey, V. Angelopoulos, S. Kurita, K. Keika, K. Seki, and I. Shinohara (2018a), Pulsating aurora from electron scattering by chorus waves, *Nature*, 554, 337-340, doi:10.1038/nature25505.

Kasahara, S., S. Yokota, T. Mitani, K. Asamura, M. Hirahara, Y. Shibano, and T. Takashima (2018b), Medium-Energy Particle experiments - electron analyser (MEP-e) for the Exploration of energization and Radiation in Geospace (ERG) mission, *Earth Planets Space*, 70, 69, doi:10.1186/s40623-018-0847-z.

Kasahara, S., S. Yokota, T. Hori, K. Keika, Y. Miyoshi, and I. Shinohara (2018c), The MEP-e instrument Level-2 3-D flux data of Exploration of energization and Radiation in Geospace (ERG) Arase satellite, DOI:10.34515/DATA.ERG-02000.

Kasahara, Y., Y. Kasaba, H. Kojima, S. Yagitani, K. Ishisaka, A. Kumamoto, F. Tsuchiya, M. Ozaki, S. Matsuda, T. Imachi, Y. Miyoshi, M. Hikishima, Y. Katoh, M. Ota, M. Shoji, A. Matsuoka, and I. Shinohara (2018a), The Plasma Wave Experiment (PWE) on board the Arase (ERG) satellite, *Earth Planets Space*, 70, 86, doi:10.1186/s40623-018-0842-4.

Kasahara, Y., Y. Kasaba, S. Matsuda, M. Shoji, T. Nakagawa, K. Ishisaka, S. Nakamura, M. Kitahara, Y. Miyoshi, and I. Shinohara (2018b), The PWE/EFD instrument Level-2 spin-fit electric field data of Exploration of energization and Radiation in Geospace (ERG) Arase satellite, DOI:10.34515/DATA.ERG-07000.

Kasahara, Y., H. Kojima, S. Matsuda, M. Ozaki, S. Yagitani, M. Shoji, S. Nakamura, M. Kitahara, Y. Miyoshi, and I. Shinohara (2018c), The PWE/OFA instrument Level-2 spectrum data of Exploration of energization and Radiation in Geospace (ERG) Arase satellite, DOI:10.34515/DATA.ERG-08000.

Kasahara, Y., A. Kumamoto, F. Tsuchiya, S. Matsuda, M, Shoji, S. Nakamura, M. Kitahara, I. Shinohara, and Y. Miyoshi (2018d), The PWE/HFA instrument Level-2 spectrum data of Exploration of energization and Radiation in Geospace (ERG) Arase satellite, DOI:10.34515/DATA.ERG-10000.

Katoh, Y., Omura, Y., Miyake, Y., Usui, H., and Nakashima, H. (2018) Dependence of generation of whistler mode chorus emissions on the temperature anisotropy and density of energetic electrons in the Earth's inner magnetosphere, *J. Geophys. Res.: Space Phys.*, 123, 1165–1177, doi.org/10.1002/2017JA024801.

Kumamoto, A., F. Tsuchiya, Y. Kasahara, Y. Kasaba, H. Kojima, S. Yagitani, K. Ishisaka, T. Imachi, M. Ozaki, S. Matsuda, M. Shoji, A. Matsuoka, Y. Katoh, Y. Miyoshi, and T. Obara (2018), High Frequency Analyzer (HFA) of Plasma Wave Experiment (PWE) onboard the Arase spacecraft, *Earth Planets Space*, 70, 82, doi:10.1186/s40623-018-0854-0.

Li, W., R. M. Thorne, J. Bortnik, Y. Nishimura, and V. Angelopoulos (2011), Modulation of whistler mode chorus waves: 1. Role of compressional Pc4–5 pulsations, *J. Geophys. Res.*, 116, A06205, doi:10.1029/2010JA016312.

Liu, N., Z. Su, Z. Gao, H. Zheng, Y. Wang, and S. Wang (2019), Magnetospheric chorus, exohiss, and magnetosonic emissions simultaneously modulated by fundamental toroidal standing Alfvén waves following solar wind dynamic pressure fluctuations, *Geophys. Res. Lett.*, 46, 1900–1910, doi:10.1029/2018GL081500.

Matsuda, S., Y. Kasahara, H. Kojima, Y. Kasaba, S. Yagitani, M. Ozaki, T. Imachi, K. Ishisaka, A. Kumamoto, F. Tsuchiya, M. Ota, S. Kurita, Y. Miyoshi, M. Hikishima, A. Matsuoka and I. Shinohara (2018), Onboard Software of Plasma Wave Experiment aboard Arase: Instrument Management and Signal Processing of Waveform Capture/Onboard Frequency Analyzer, *Earth Planets Space*, 70, 75, doi:10.1186/s40623-018-0838-0.

Matsuoka, A., M. Teramoto, R. Nomura, M. Nosé, A. Fujimoto, Y. Tanaka, M. Shinohara, T. Nagatsuma, K. Shiokawa, Y. Obana, Y. Miyoshi, M. Mita, T. Takashima, and I. Shinohara (2018a), The ARASE(ERG) magnetic field investigation, *Earth Planets Space*, 70, 43, doi:10.1186/s40623-018-0800-1.

Matsuoka, A., M. Teramoto, S. Imajo, S. Kurita, Y. Miyoshi, and I. Shinohara (2018b), The MGF instrument Level-2 spinfit magnetic field data of Exploration of energization and Radiation in Geospace (ERG) Arase satellite, DOI:10.34515/DATA.ERG-06001.

McIlwain, C. E. (1961), Coordinates for mapping the distribution of magnetically trapped particles, *J. Geophys. Res.*, 66, 3681-3691, doi:10.1029/JZ066i011p03681.

Mitani, T., T. Takashima, S. Kasahara, W. Miyake and M. Hirahara (2018a), High-energy electron experiments (HEP) aboard the ERG (Arase) satellite, *Earth, Planets and Space*, 70, 77, doi:10.1186/s40623-018-0853-1.

Mitani, T., T. Hori, I. Park, T. Takashima, Y. Miyoshi, and I. Shinohara (2018b), The HEP instrument Level-2 omni-directional flux data of Exploration of energization and Radiation in Geospace (ERG) Arase satellite, DOI:10.34515/DATA.ERG-01001, 2018.

Miyoshi, Y., and R. Kataoka (2011), Solar cycle variations of outer radiation belt and its relationship to solar wind structure dependences, *J. Atmos. Sol-Terr. Phys.*, 73, 1, 77-87, doi:10.1016/j.jastp.2010.09.031.

Miyoshi, Y., Y. Katoh, T. Nishiyama, T. Sakanoi, K. Asamura, and M. Hirahara, Time of flight analysis of pulsating aurora electrons, considering wave-particle interactions with propagating whistler mode waves, J. Geophys. Res., 115, A10312, doi:10.1029/2009JA015127, 2010.

Miyoshi, Y., R. Kataoka, Y. Kasahara, A. Kumamoto, T. Nagai, and M. Thomsen, High-speed solar wind with southward interplanetary magnetic field causes relativistic electron flux enhancement of the outer radiation belt via enhanced condition of whistler waves, Geophys. Res. Lett., 40, doi:10.1002/grl.50916, 2013.

Miyoshi, Y. S. Saito, K.Seki, T. Nishiyama, R. Kataoka, K. Asamura, Y. Katoh, Y. Ebihara, T. Sakanoi, M. Hirahara, S. Oyama, S. Kurita, and O. Santolik, Relation between energy spectra of pulsating aurora electrons and frequency spectra of whistler-mode chorus waves, J. Geophys. Res., 120, 7728-7736, doi:10.1002/2015JA021562, 2015.

Miyoshi, Y., I. Shinohara,, T. Takashima, K. Asamura, N. Higashio, T. Mitani, S. Kasahara, S. Yokota, Y. Kazama, S.-Y. Wang, S. W. Tam, P. T. P Ho, Y. Kasahara, Y. Kasaba, S. Yagitani, A. Matsuoka, H. Kojima, H. Katoh, K. Shiokawa, and K. Seki (2018a), Geospace Exploration Project ERG, *Earth Planets Space*, 70, 101, doi:10.1186/s40623-018-0862-0.

Miyoshi, Y., T. Hori, M. Shoji, M. Teramoto, T. F. Chang, S. Matsuda, S. Kurita, T. Segawa, N. Umemura, K. Keika, Y. Miyashita, Y. Tanaka, N. Nishitani, T. Takashima, and I. Shinohara (2018b), The ERG Science Center, *Earth Planets Space*, 70, 96, doi:10.1186/s40623-018-0867-8.

Miyoshi, Y., I. Shinohara and C.-W. Jun (2018c), The Level-2 orbit data of Exploration of energization and Radiation in Geospace (ERG) Arase satellite, 10.34515/DATA.ERG-12000.

Miyoshi, Y., K. Hosokawa, S. Kurita, S.-I. Oyama, Y. Ogawa, S. Saito, I. Shinohara, A. Kero, E. Turunen, P. T. Verronen, S. Kasahara, S. Yokota, T. Mitani, T. Takashima, N. Higashio, Y. Kasahara, S. Masuda, F. Tsuchiya, A. Kumamoto, A. Matsuoka, T. Hori, K. Keika, M. Shoji, M. Teramoto, S. Imajo, C. Jun, and S. Nakamura (2021), Penetration of MeV electrons into the mesosphere accompanying pulsating aurorae, Scientific Reports, 11, 13724, doi:10.1038/s41598-021-92611-3.

Nishimura, Y., J. Bortnik, W. Li, R. M. Thorne, L. R. Lyons, V. Angelopoulos, S. B. Mende, J. W. Bonnell, O. Le Contel, C. Cully, R. Ergun, U. Auster (2010), Identifying the Driver of Pulsating Aurora, *Science*, 330, 81-84, doi:10.1126/science.1193186.

Omura, Y. (2021), Nonlinear wave growth theory of whistler-mode chorus and hiss emissions in the magnetosphere, *Earth Planets Space*, 73, 95, doi:10.1186/s40623-021-01380-w.

Omura, Y., Y. Katoh, and D. Summers (2008), Theory and simulation of the generation of whistler-mode chorus, *J. Geophys. Res.*, 113, A04223, doi:10.1029/2007JA012622.

Omura, Y., M. Hikishima, Y. Katoh, D. Summers, and S. Yagitani (2009), Nonlinear mechanisms of lower-band and upper-band VLF chorus emissions in the magnetosphere, *J. Geosphys. Res.*, 114, A07217, doi:10.1029/2009JA014206.

Ozaki, M., S. Yagitani, Y. Kasahara, H. Kojima, Y. Kasaba, A. Kumamoto, F. Tsuchiya, S. Matsuda, A. Matsuoka, T. Sasaki, and T. Yumoto (2018), Magnetic Search Coil (MSC) of Plasma Wave Experiment (PWE) aboard the Arase (ERG) satellite, Earth Planets Space, 70, 76, doi:10.1186/s40623-018-0837-1.

Southwood, D. J., J. W. Dungey, and R. J. Etherington (1969), Bounce resonant interaction between pulsations and trapped particles, *Planet. Space Sci.*, 17, 349-361.

Southwood, D. J., and M. G. Kivelson (1981), Charged Particle Behavior in Low-Frequency Geomagnetic Pulsations 1. Transverse Waves, *J. Geosphys. Res.*, 86, 5643-5655.

Takahashi, K. (2016), ULF waves in the inner magnetosphere. In A. Keiling, D.-H. Lee, & V. Nakariakov (Eds.), Low-frequency waves in space plasmas (pp. 51–63). https://doi.org/10.1002/9781119055006.ch4

Takahashi, K., C. Z. Cheng, R. W. McEntire, and L. M. Kistler (1990), Observation and theory of Pc 5 waves with harmonically related transverse and compressional components, *J. Geosphys. Res.*, 95(A2), 977-989.

Takahashi, K., B. J. Anderson, and S. Ohtani (1996), Multisatellite study of nightside transient toroidal waves, *J. Geosphys. Res.h*, 101, 24,815-24,825, doi:10.1029/96JA02045.

Takahashi, K., K.-H. Glassmeier, V. Angelopoulos, J. Bonnell, Y. Nishimura, H. J. Singer, and C. T. Russell (2011), Multisatellite observations of a giant pulsation event, J. Geophys. Res., 116, A11223, doi:10.1029/2011JA016955.

Tsurutani, B. T., W. D. Gonzalez, A. L. C. Gonzalez, F. L. Guarnieri, N. Gopalswamy, M. Grande, Y. Kamide, Y. Kasahara, G. Lu, I. Mann, R. McPherron, F. Soraas, V. Vasyliunas (2006), Corotating solar wind streams and recurrent geomagnetic activity: A review, *J. Geosphys. Res.*, 111, A07S01, doi:10.1029/2005JA011273.

Tsyganenko, N. A., and M. I. Sitnov (2005), Modeling the dynamics of the inner magnetosphere during strong geomagnetic storms, *J. Geosphys. Res.*, 110, A03208, doi: 10.1029/2004JA010798.

Walt, M. (1994). Introduction to Geomagnetically Trapped Radiation (Cambridge Atmospheric and Space Science Series). Cambridge: Cambridge University Press. doi:10.1017/CBO9780511524981.

Xia, Z., L. Chen, L. Dai, S. G. Claudepierre, A. A. Chan, A. R. Soto-Chavez, and G. D. Reeves (2016), Modulation of chorus intensity by ULF waves deep in the inner magnetosphere, *Geophys. Res. Lett.*, 43, 9444–9452, doi:10.1002/2016GL070280.

Zhang, X.-J., L. Chen, A. V. Artemyev, V. Angelopoulos, and X. Liu (2019) Periodic excitation of chorus and ECH waves modulated by ultralow frequency compressions, *J. Geosphys. Res.*, 124, 8535-8550, doi:10.1029/2019JA027201.

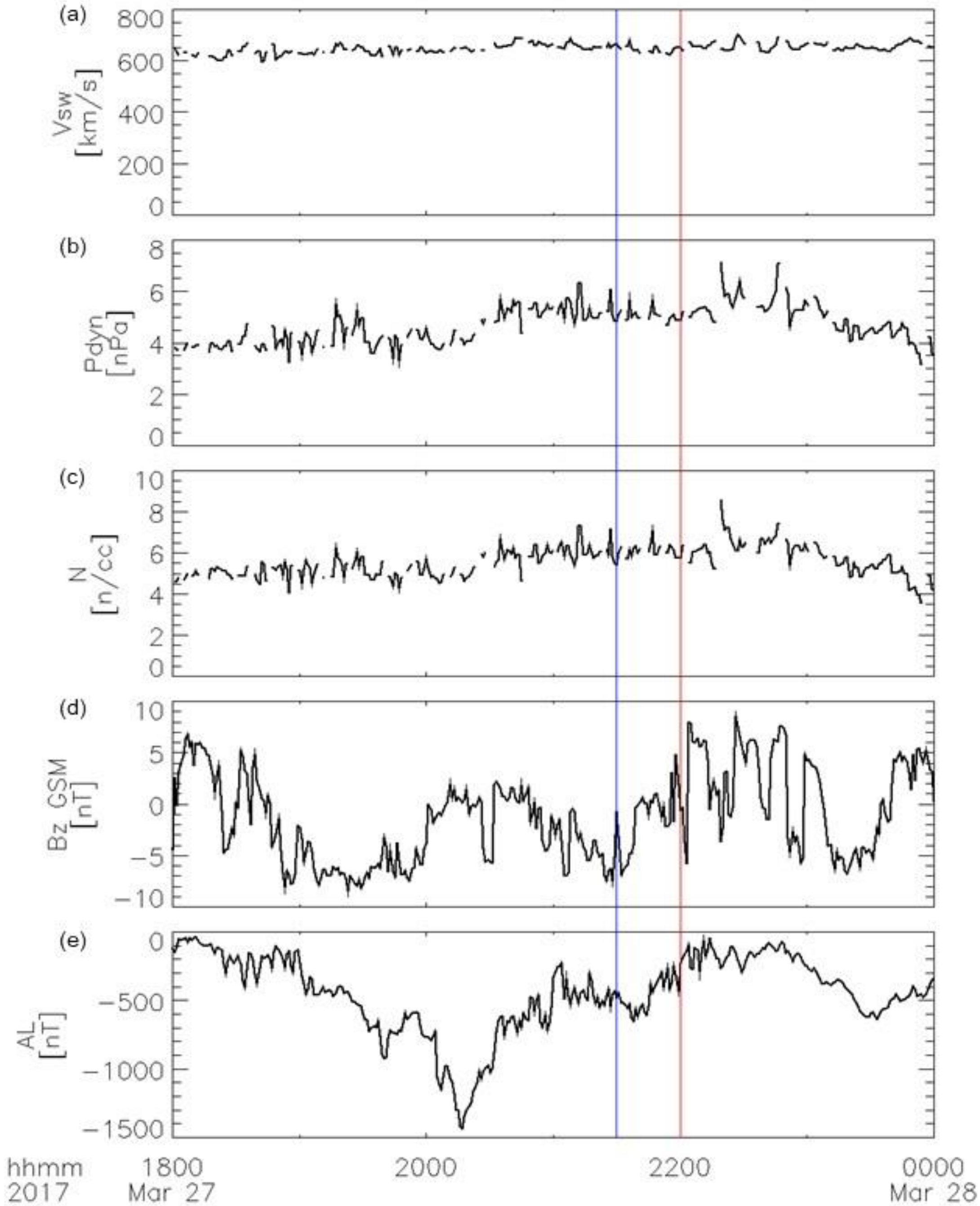

Figure 1. The time series of (a) the solar wind speed, (b) the dynamic pressure, (c) the density, (d) the Bz component of Interplanetary Magnetic Field (IMF) in the Geocentric Solar Magnetospheric (GSM) coordinate system, and (e) AL index from 18:00 UT to 24:00UT on March 27, 2017. Blue and red vertical lines indicate the start and end time of the time interval shown in Figure 2, respectively.

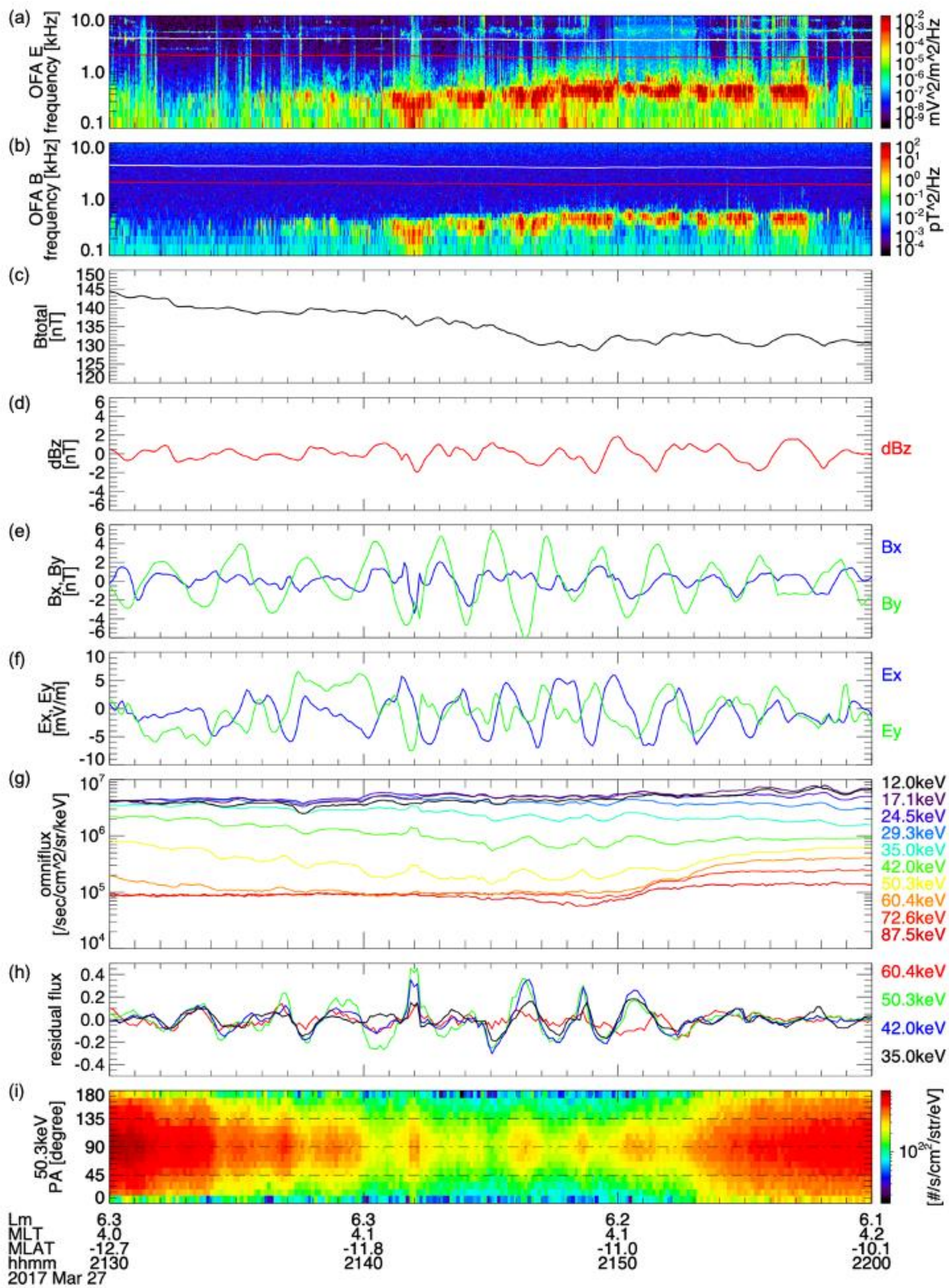
(a)
OFA E frequency [kHz]
mV^2/m^2/Hz
(b)
OFA B frequency [kHz]
pT^2/Hz
(c)
Btotal [nT]
(d)
dBz [nT]
dBz
(e)
Bx, By [nT]
Bx
By
(f)
Ex, Ey [mV/m]
Ex
Ey
(g)
omniflux [/sec/cm^2/sr/keV]
12.0keV
17.1keV
24.5keV
29.3keV
35.0keV
42.0keV
50.3keV
60.4keV
72.6keV
87.5keV
(h)
residual flux
60.4keV
50.3keV
42.0keV
35.0keV
(i)
50.3keV PA [degree]
[#/s/cm²/str/eV]
Lm 6.3 6.3 6.2 6.1
MLT 4.0 4.1 4.1 4.2
MLAT -12.7 -11.8 -11.0 -10.1
hhmm 2130 2140 2150 2200
2017 Mar 27

499

Figure 2. Observation results of the ERG satellite from 21:30 UT to 22:00 UT on March 27, 2017. (a) Wave electric field and (b) magnetic field spectra observed by the OFA of the PWE along with the f_{ce} (shown in white) and the $0.5f_{ce}$ (red) calculated from the magnetic field data from the MGF. (c) The total magnetic field intensity. (d) The Bz, (e) Bx (blue), and By (green) components of the magnetic field in the MFA coordinate system. (f) The Ex (blue) and Ey (green) components of the electric field in the MFA coordinate system. (g) The omnidirectional electron fluxes from 12.0 to 87.5 keV energy range. (h) the residual fluxes calculated from the omnidirectional electron number fluxes in the 35.0 keV (black), 42.0 keV (blue), 50.3 keV (green), and 60.4 keV (red) energy range. (i) The pitch angle distribution in the 50.3 keV energy range observed by the MEP-e.

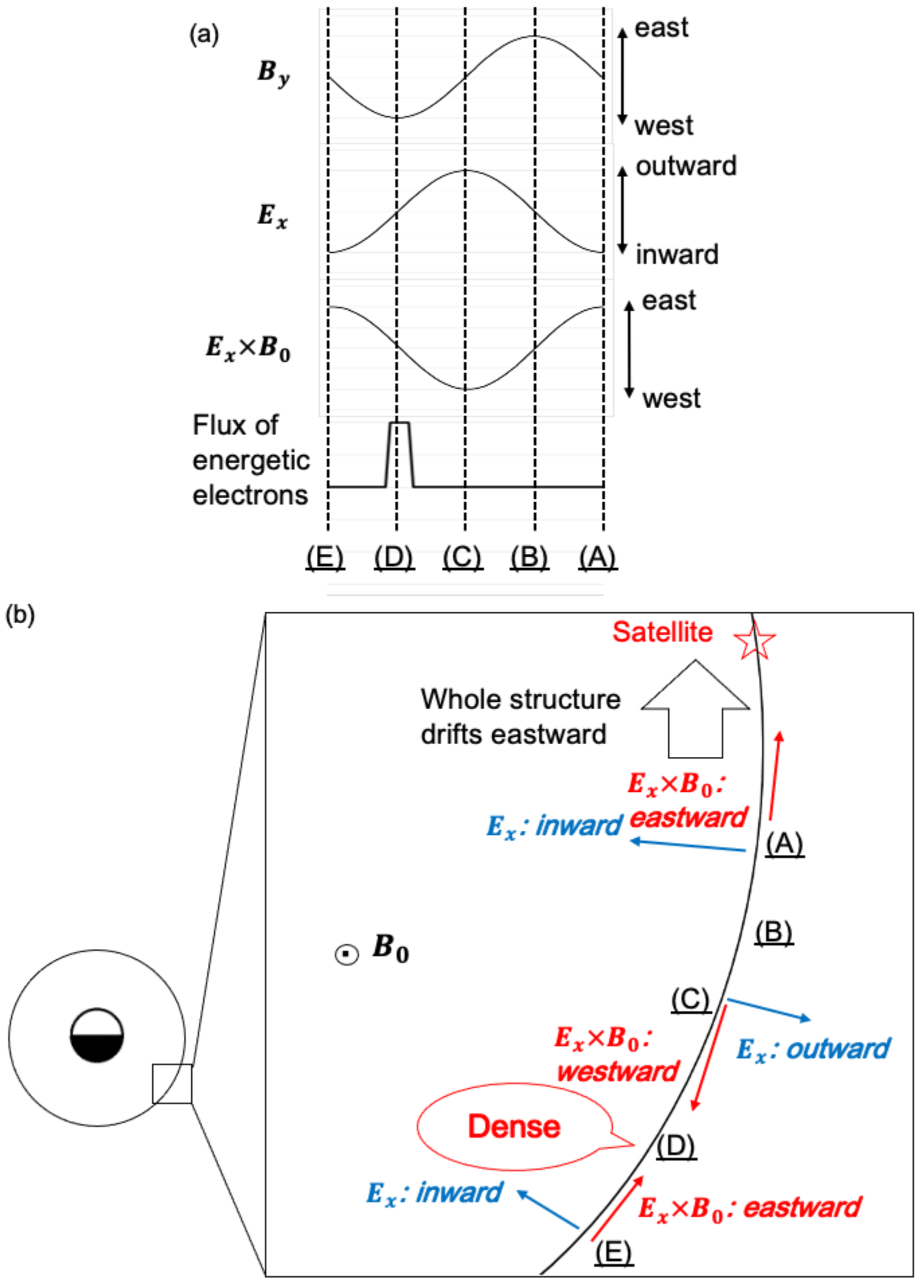

Figure 3. Schematic illustration of (a) the phase relationship among the wave electromagnetic field of toroidal mode standing ULF waves, the $\boldsymbol{E_X} \times \boldsymbol{B_0}$ drift caused by the wave electric field and the ambient magnetic field, and the fluctuation components of energetic electrons observed and expected to be observed by the satellite and (b) expected spatial structure along the drift path of energetic electrons looked down from north of the Earth.

AGU PUBLICATIONS

Geophysical Research Letters

Supporting Information for

Modulation of the energetic electron distribution caused by toroidal mode ULF waves in association with periodic enhancement of whistler-mode chorus emissions

A. Ono[1], Y. Katoh[1], M. Teramoto[2], T. Hori[3], A. Kumamoto[1], F. Tsuchiya[1], Y. Kasaba[1], K. Isono[1], Y. Miyoshi[3], S. Kasahara[4], Y. Kasahara[5], S. Matsuda[5], S. Nakamura[3], A. Matsuoka[6], S. Yokota[7], K. Keika[4], T. Mitani[8], I. Shinohara[8]

[1]Graduate School of Science, Tohoku University, JAPAN

[2] Kyushu Institute of Technology, JAPAN

[3] Nagoya University, JAPAN

[4] University of Tokyo, JAPAN

[5] Kanazawa University, JAPAN

[6] Kyoto University, JAPAN

[7] Osaka University, JAPAN

[8] ISAS/JAXA, JAPAN

Contents of this file

Introduction

This paper uses data from multi-instruments aboard the ERG (Arase) satellite. These supplementary materials are included to indicate the properties of observed whistler-mode chorus emissions (Figure S1) and the behavior of electrons in the energy range from 12 keV to 553 keV (Figures S2 and S3).

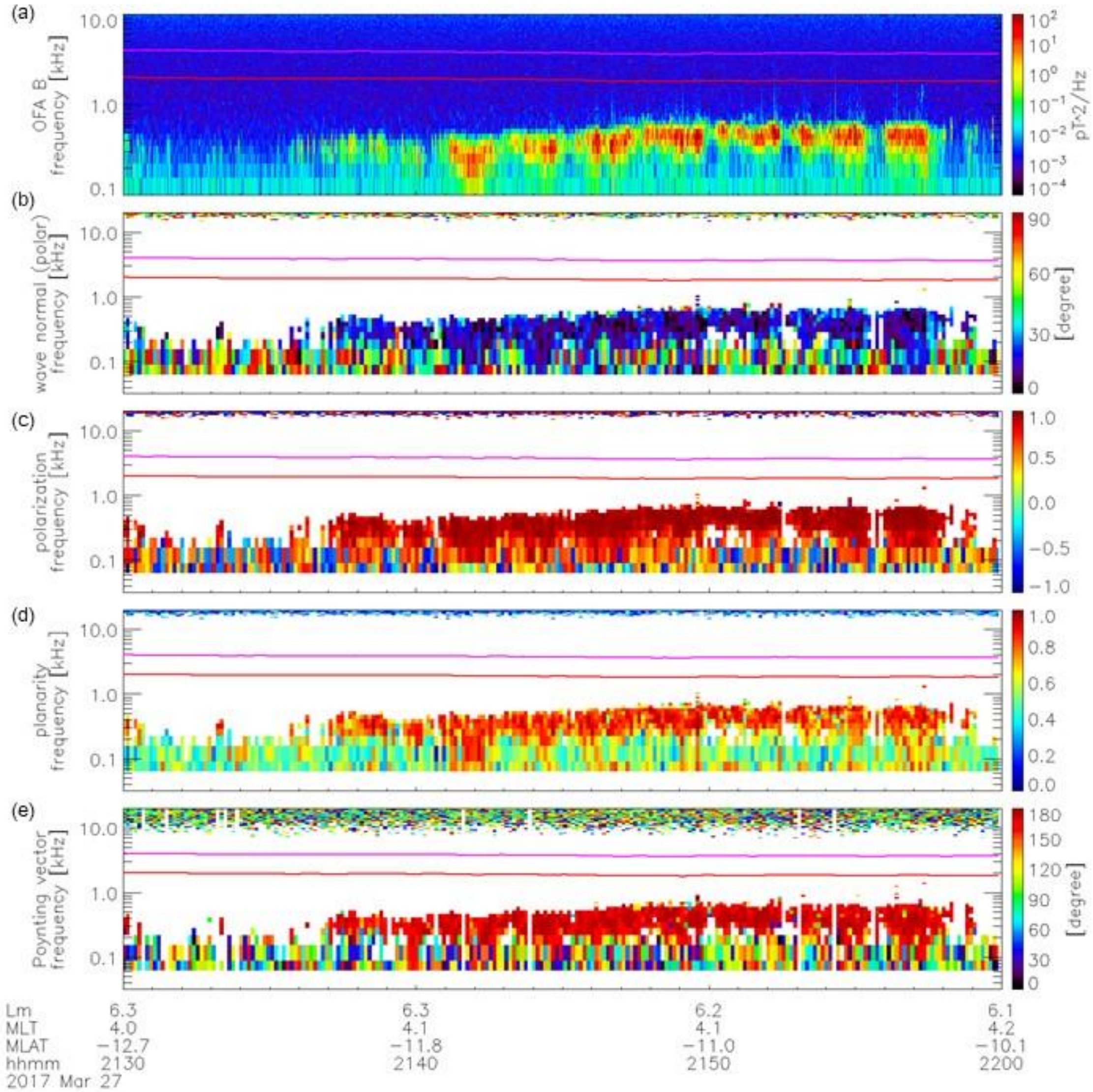

Figure S1. (a) The wave magnetic field spectrum, (b) the wave normal angle direction, (c) the polarization, (d) the planarity, and (e) the Poynting flux direction calculated from the observation results of PWE/OFA.

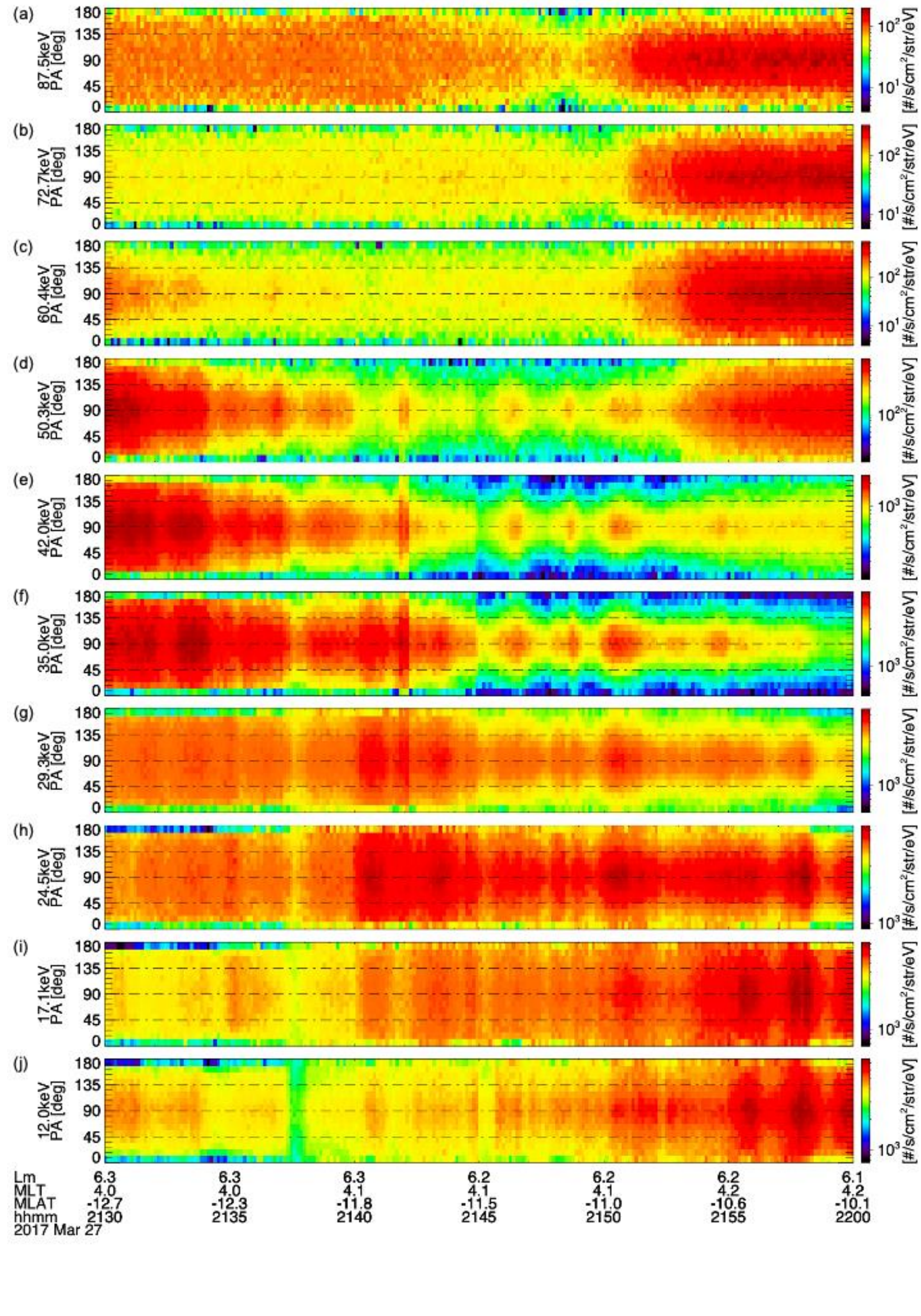

Figure S2. The pitch angle distributions in (a) 87.5 keV, (b) 72.7 keV, (c) 60.4 keV, (d) 50.3 keV, (e) 42.0 keV, (f) 35.0 keV, (g) 29.3 keV, (h) 24.5 keV, (i) 17.1 keV and (j) 12.0 keV energy range observed by MEP-e.

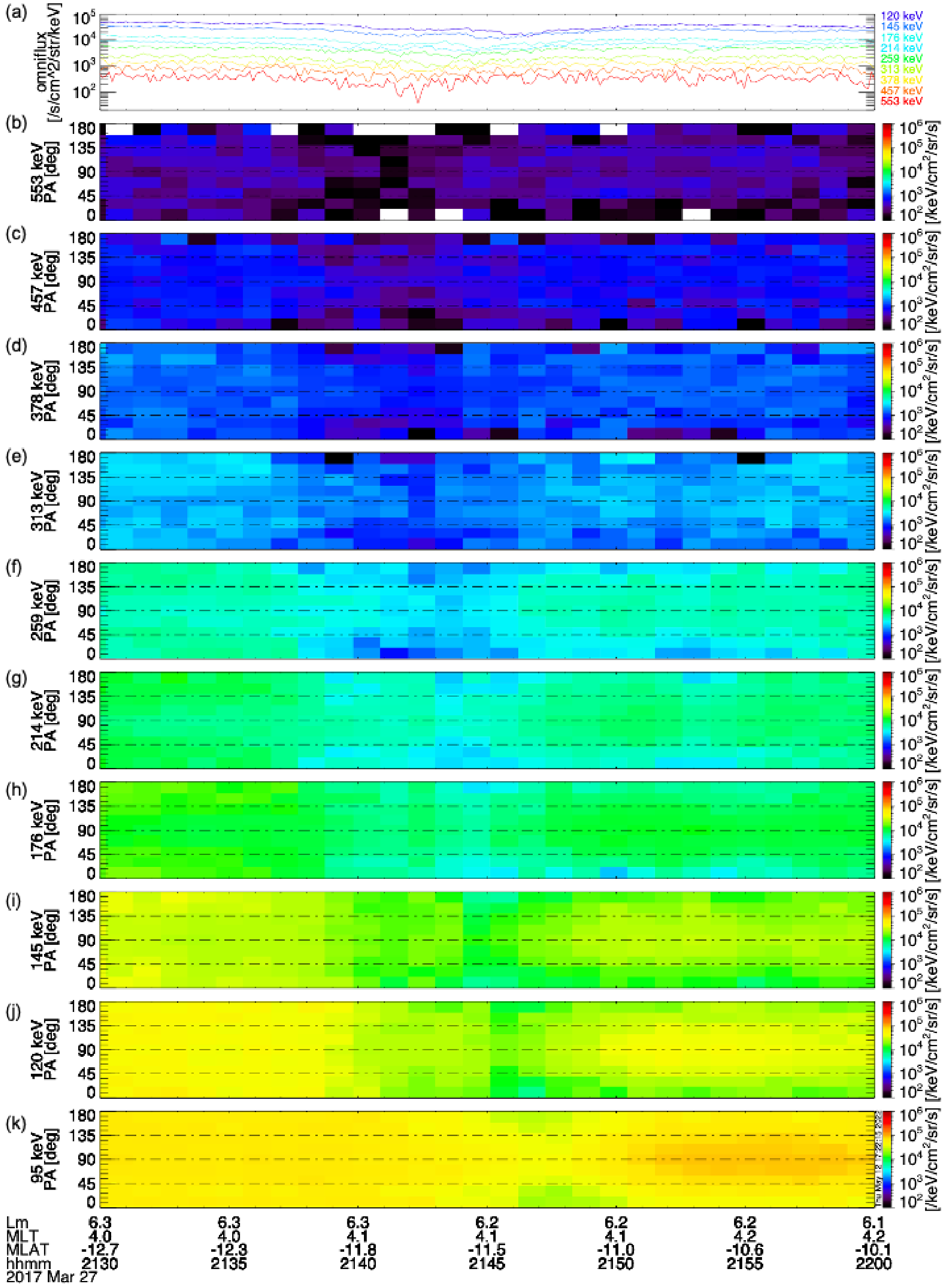
(a)
omniflux
[/s/cm^2/str/keV]
120 keV
145 keV
176 keV
214 keV
259 keV
313 keV
378 keV
457 keV
553 keV
(b)
553 keV
PA [deg]
(c)
457 keV
(d)
378 keV
(e)
313 keV
(f)
259 keV
(g)
214 keV
(h)
176 keV
(i)
145 keV
(j)
120 keV
(k)
95 keV
[/keV/cm^2/sr/s]
Lm
MLT
MLAT
hhmm
2017 Mar 27

Figure S3. (a) The omni-directional electron differential fluxes in the energy range from 120 keV to 554 keV energy range, and the pitch angle distributions in (b) 553 keV, (c) 457 keV, (d) 378 keV, (e) 313 keV, (f) 259 keV, (g) 214 keV, (h) 176 keV, (i) 145 keV, (j) 120 keV, and (k) 95 keV energy range observed by HEP.